Journal of Power Sources 196 (2011) 7217–7224

Contents lists available at ScienceDirect

Journal of Power Sources

journal homepage: www.elsevier.com/locate/jpowsour

Studying the $CO–CO_2$ characteristics of SOFC anodes by means of patterned Ni anodes

A. Utz [a,*], A. Leonide [a], A. Weber [a], E. Ivers-Tiffée [a,b]

[a] Karlsruher Institut für Technologie (KIT), Institut für Werkstoffe der Elektrotechnik (IWE), Adenauerring 20b, D-76131 Karlsruhe, Germany
[b] DFG Center for Functional Nanostructures (CFN), Karlsruhe Institute of Technology (KIT), D-76131 Karlsruhe, Germany

ARTICLE INFO

Article history:
Received 30 June 2010
Received in revised form 5 October 2010
Accepted 18 October 2010
Available online 26 October 2010

Keywords:
SOFC
Patterned Ni anodes
CO/CO_2

ABSTRACT

The high potential of solid oxide fuel cells (SOFC) arises due to the high degree of efficiency and fuel flexibility. However, the elementary kinetic steps of the anodic processes taking place at the boundary of electrolyte–anode–gas are still largely unknown. Patterned Ni anodes on Y_2O_3-stabilized ZrO_2 are regarded as a promising method to determine these kinetics.

In analogy to our previous study with patterned Ni anodes for the $H_2–H_2O$ system, this study is systematically devoted to the elementary kinetics of the CO electrochemical oxidation in $CO–CO_2$ gas mixtures. Data analysis is backed by extensive knowledge on patterned anode stability and dynamics gained during previous studies. The electrochemical characterization is performed for a large parameter variation range (pCO_2, pCO and T) by electrochemical impedance spectroscopy.

Contrary to the characterization in $H_2–H_2O$ atmosphere no slow relaxation processes were observed and the degradation rate is smaller. Changes in parameter dependency over the investigated parameter range indicate different reaction mechanisms as a function of gas composition. Only slightly higher polarization losses are observed for CO oxidation compared to H_2. The comparison of the results from patterned anodes to high-performance Ni/8YSZ cermet anodes employed in anode supported cells yields good agreement.

1. Introduction

The knowledge of the actual elementary kinetic steps of the electrochemical oxidation at solid oxide fuel cell (SOFC) anodes is considered to be key to further improvements of the anodic performance [1]. Several reaction mechanisms have been proposed for the oxidation of H_2 as well as CO; an overview is given in [2]. Even though both experimental and modeling studies have been performed for the two atmospheres, the elementary kinetic steps are still not clear.

In systems with a purely electron conducting electrode and ionic conducting electrolyte the electrooxidation is restricted to the triple phase boundary (TPB) of electrode, electrolyte and gas phase [1]. Hence, model Ni anodes with a well-defined Ni structure on the YSZ electrolyte are advantageous for the investigation of the reaction kinetics. Among them are point-, grid- and patterned anodes, for an overview see [3]. Patterned anodes exhibit a well defined and a well approachable triple phase boundary length (l_{TPB}) and are therefore chosen in this study.

Several studies on electrooxidation, which are based on patterned Ni anodes, have been performed so far for the $H_2–H_2O$ atmosphere [4–8]. In the most recent study, our group could attribute the observed discrepancies considering absolute values of the line specific resistance (LSR) and controversial parameter dependencies to different degradation and relaxation processes occurring during characterization of nominally stable patterned Ni anodes [8]. The results of characterization in $H_2–H_2O$ atmosphere indicate a hydrogen spillover mechanism [3,8,9].

The mechanism of electrooxidation of CO in $CO–CO_2$ atmospheres is less understood. Several studies have been performed with Ni/8YSZ anodes and Ni point anodes [10–19], however only one study is reported for patterned Ni anodes [20]. Again some controversy exists regarding the reaction mechanisms and the dependency of polarization resistance on fuel composition, the details are discussed in Section 2. Therefore, in this study the behavior of patterned Ni anodes in $CO–CO_2$ atmosphere is studied in detail. The parameter dependencies of partial pressures of CO and CO_2 (pCO and pCO_2 respectively) as well as temperature (T) are determined under consideration of degradation and relaxation mechanisms. A comparison to the results from characterization of high-performance Ni/8YSZ cermet anodes employed in anode supported cells (ASC) [17] as well as of Ni grid electrodes [11] is given.

* Corresponding author. Tel.: +49 721 608 7769; fax: +49 721 608 7492.
E-mail address: annika.utz@kit.edu (A. Utz).

0378-7753/$ – see front matter © 2010 Elsevier B.V. All rights reserved.
doi:10.1016/j.jpowsour.2010.10.056

2. Related work

A general discussion is whether different mechanisms apply for the electrochemical oxidation in H_2–H_2O and CO–CO_2 atmospheres: whereas several studies state that the anodic reaction is not affected by the kind of fuel but only by the partial pressure of oxygen (pO_2) and hence the reaction mechanisms are similar in both atmospheres [12,18] other studies report a 2–10 times higher polarization resistance for CO–CO_2 atmospheres compared to H_2–H_2O [10,11,14,15,19–21]. In an early study, Etsell characterized porous Pt anodes in CO–CO_2 atmosphere and found that two species are involved in the reaction. However, no definite conclusion was possible whether gaseous or adsorbed CO was involved besides gaseous CO_2 [13]. The maximum exchange current density is obtained at around 50% CO; this observation was affirmed by Aaberg in a study with Ni/8YSZ cermet electrodes [10]. A combined modeling and experimental study has been performed by Lauvstad including four different reaction mechanisms [15,21]. The results of experimental analysis with Ni point anodes indicate a reaction mechanism involving at least two adsorbed intermediates that were assumed to be O_{ad} and CO_{ad}.

Etsell gives two explanations for the lower exchange current densities in CO–CO_2 mixtures than in H_2–H_2O mixtures: (i) the exchange current density was found to be inversely proportional to the number of free surface sites θ_{CO} which generally prevails θ_H due to higher enthalpy of adsorption of CO; (ii) higher energy barriers impede the electrochemical reaction of CO [13].

Most studies do not determine the reaction orders as either pCO or pCO$_2$ are varied simultaneously [10] or too few gas phase compositions are used to determine the quantitative dependency [15]. So far, the parameter dependencies of pCO, pCO$_2$ and T have only been determined by Boulenouar with Ni grid electrodes [11] and our group with Ni/8YSZ cermet anodes [17]. Boulenouar reports a coefficient of 0.5 for both pCO$_2$ and pCO variation [11]. In contrast, we determined a value of +0.25 for pCO$_2$ variation and −0.06 for pCO variation [17]; the same qualitative behavior is reported by Lauvstad et al. [15].

The only study with patterned Ni anodes in CO–CO_2 atmosphere reported so far is by Sukeshini et al. [20]. The patterned Ni anodes have ended up as separate Ni islands after testing; with an indefinable triple phase boundary length. This result clearly demonstrates that structural changes during experiments have to be taken into account. Unfortunately, the course of the polarization resistance with time was not measured and a variation of pCO, pCO$_2$ and T was not included. For this reason, no quantitative parameter dependencies can be extracted from this study. However, it can be retained that the polarization resistance in H_2–H_2O atmosphere is below values obtained in CO–CO_2 atmosphere. Furthermore, the dominance of H_2 oxidation during the oxidation of CO–H_2 mixtures has been shown for patterned anodes [20]. This is in agreement with our findings for Ni/8YSZ cermet anodes [19].

3. Experimental

3.1. Sample preparation

Patterned Ni anodes with an area of 10.25 mm × 10.25 mm were fabricated on 8.5 mol% polycrystalline Y_2O_3-stabilized ZrO_2 (YSZ) substrates (Itochu Ceratec Corp., Japan) using a standard photolithography process [22], the procedure is described in our previous study [8]. The design of the pattern is composed of an area of 9.25 mm × 9.25 mm with parallel Ni stripes; in this study stripes with 25 μm width, a spacing of 160 μm and a thickness of 800 nm are chosen. In a previous study, this thickness has been found to ensure the stability of the structure during characterization at temperatures of up to 800 °C in reducing atmosphere [23]. An additional frame with 500 μm width assures the contacting of all stripes, see Fig. 1. This design yields a triple phase boundary length $l_{TPB,th}$ of 1 m. Pre test SEM analysis shows a perfect pattern, e.g. no stripes are destroyed or delaminated.

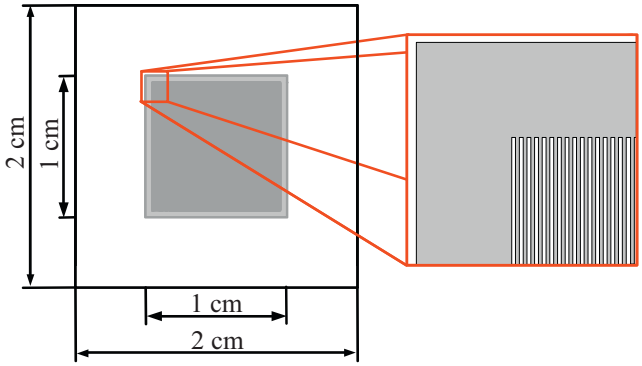

Fig. 1. Scheme of design of patterned Ni anodes. The Ni pattern is of size 10.25 mm × 10.25 mm positioned in the centre of the 2 cm × 2 cm 8YSZ substrate. The design consists of stripes with different widths and spacings. A 500 μm wide frame assures electrical contacting of all stripes and allows the use of a special contact block, see Fig. 2.

To circumvent the unavoidable distortions of the impedance caused by reference electrodes [24], a Ni/8YSZ cermet anode exhibiting an at least 2 orders of magnitude lower polarization resistance was chosen as the counter electrode. The counter electrodes were applied before preparation of the patterned Ni anodes, as sintering and reduction of this anode require the highest temperatures.

3.2. Measurement setup

The contacting of both working and counter electrode has been modified compared to the setup in our previous study [8]: the patterned Ni anode is contacted by a special contact block that is positioned on two sides of the frame perpendicular to the stripe pattern, see Fig. 2. A fine Ni mesh on the contact surface ensures uniform contacting. The counter electrode is contacted by a combination of a fine and coarse Ni mesh on a Ni sample holder with flow field. These modifications allow a direct gas flow to the patterned Ni anode as well as improved gas supply to the counter electrode. Hence, it was possible to reduce the influence of gas diffusion on overall electrode performance.

The Ni sample holder was then placed in a gastight Al_2O_3 chamber where the sample was purged with the appropriate fuel gas composition on both sides. The fuel gas composition was controlled

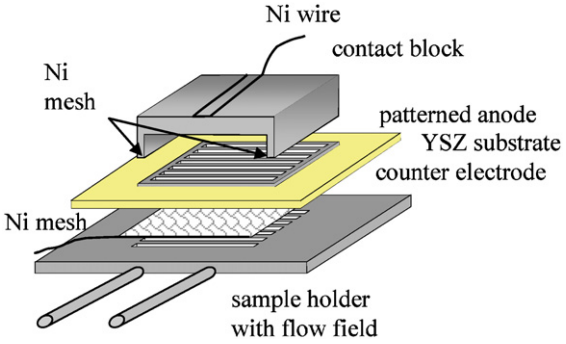

Fig. 2. Scheme of measurement setup. The patterned Ni anode is contacted by the combination of a fine Ni mesh on the interface of the special Ni contact block. The Ni/8YSZ cermet anode is contacted by a combination of fine and coarse Ni mesh and positioned onto a Ni sample holder with flow field (channel width 1 mm).

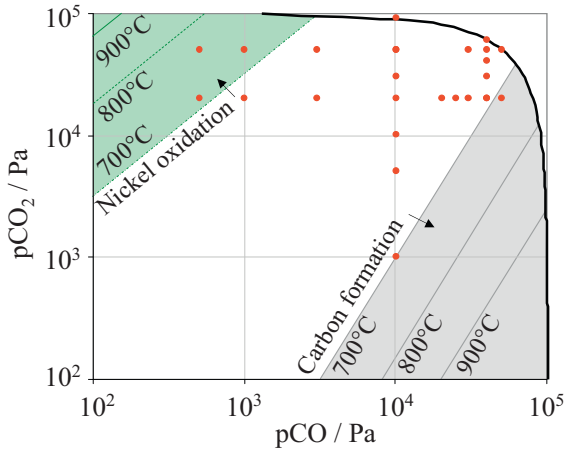

Fig. 3. Summary of parameter variation range of pCO and pCO$_2$ realized in this study together with the critical regions of carbon formation as well as oxidation of Ni for temperatures of 700, 800 and 900 °C.

by mass flow controllers that allow a variation of pCO, pCO$_2$ and pN$_2$ in between 0 and 100% (gas flow 300 ml min^{-1}); N$_2$ is used as balance for independent variation of pCO and pCO$_2$ respectively. A Nernst probe located near the sample monitors the p(O$_2$) and hence provides information about the actual gas composition and possible leakages in the setup, which were very low (<0.02%) in this and our previous study [8].

3.3. Electrochemical characterization

For the electrochemical characterization, electrochemical impedance spectra (EIS) are recorded for parameter variation of pCO, pCO$_2$ and temperature. For the choice of gas variation range two restrictions need to be considered: (i) oxidation of Ni at elevated oxygen partial pressures following the oxidation reaction (Eq. (1)); (ii) solid carbon formation at high concentrations of CO following the Boudouard reaction (Eq. (2)) and subsequent metal dusting of Ni [25].

$$\mathrm{Ni} + \frac{1}{2}\mathrm{O_2} \rightleftharpoons \mathrm{NiO} \quad (1)$$

$$2\mathrm{CO} \rightleftharpoons \mathrm{C} + \mathrm{CO_2} \quad (2)$$

The range of parameter variation of pCO and pCO$_2$ that avoids both effects was calculated using the thermodynamic database MALT [26] and is indicated for temperatures of 700–900 °C in Fig. 3. In this study, two series of gas variation of pCO and pCO$_2$ respectively were realized with up to 9 points per series, see Fig. 3; N$_2$ was used as balance. The following variations have been performed: 4.0×10^2 Pa $\leq p\mathrm{CO} \leq 5.1 \times 10^4$ Pa and 9.5×10^2 Pa $\leq p\mathrm{CO_2} \leq 9.2 \times 10^4$ Pa resulting in $8\% \leq \beta_{\mathrm{CO/CO_2}} \leq 99\%$; 700 °C $\leq T \leq$ 800 °C. In this context $\beta_{\mathrm{CO/CO_2}}$ is determined according to the relative water vapor content in H$_2$–H$_2$O atmosphere following the equation: $\beta_{\mathrm{CO/CO_2}} = p\mathrm{CO_2}/(p\mathrm{CO} + p\mathrm{CO_2})$.

The recording of impedance spectra was performed by a Solartron 1260 FRA, in a frequency range of 100 mHz to 1 MHz. Due to the high impedance of the patterned anodes voltage stimulus was chosen instead of current stimulus; the amplitude was 10 mV.

To investigate the parameter dependency of the charge transfer polarization, series of impedance measurements were carried out in which only one cell parameter at a time was varied (pCO, pCO$_2$and T). Accounting for the degradation and relaxation processes observed for patterned Ni anodes during characterization in H$_2$–H$_2$O atmosphere [8], the relaxation behavior upon gas composition changes as well as the degradation rate were examined.

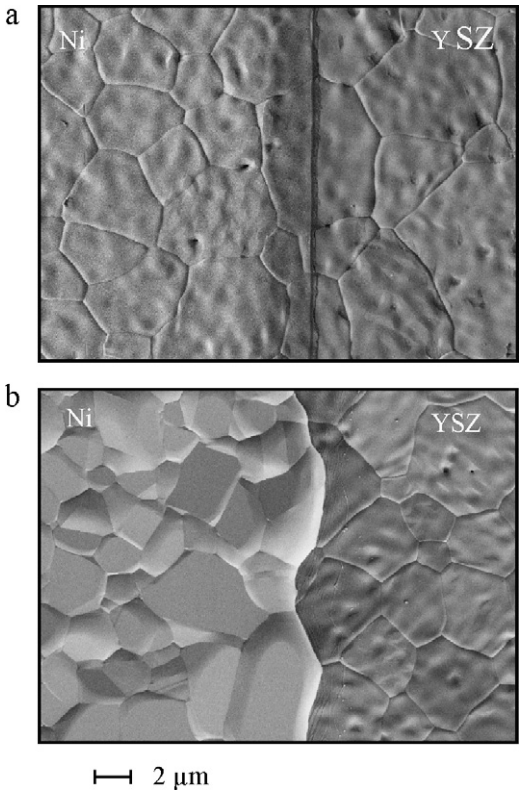

Fig. 4. SEM images of patterned Ni anodes: (a) as prepared and (b) after characterization at 800 °C for varying gas compositions of pCO and pCO$_2$. The increase in l_{TPB} is accounted for by a correction factor of $\tau_{\mathrm{corr}} = 1.3$.

4. Results and discussion

4.1. Impedance spectra and line specific resistance

Our previous study showed that three processes are contributing to the overall impedance response [8]: besides the charge transfer process of the patterned Ni anode, contributions of gas diffusion and the counter electrode are detected. For the interpretation of impedance spectra, the same equivalent circuit is used. It consists of three RQ elements in series with additional ohmic contributions of electrolyte and measurement setup and an inductive element accounting for the wiring.

The line specific resistance (LSR) is calculated from Eq. (3) as the product of polarization resistance R_{pol}, electrode area A and triple phase boundary length per electrode area l_{TPB}. The notation LSR refers to the entire polarization resistance including contributions of gas diffusion and counter electrode; in the case that only the contribution of the charge transfer process (R_{ct}) is considered the notation is LSR$_{\mathrm{ct}}$.

$$\mathrm{LSR} = R_{\mathrm{pol}} \cdot A \cdot l_{\mathrm{TPB}} \quad (3)$$

The l_{TPB} of each sample was determined individually and takes into account a correction factor $\tau_{\mathrm{corr}} = 1.3$ introduced by geometric rearrangements (i.e. grain growth) during characterization at $T = 800$ °C, see Fig. 4. In our previous stability study we found that the Ni structure is subject to considerable temperature dependent morphological changes during the first 20 h of thermal exposure at 800 °C with consecutive stabilization [23]. Therefore, in order to assure a reproducible starting point for the characterization of patterned Ni anodes, the same standard initial heat treatment than for characterization in H$_2$–H$_2$O atmosphere has been applied prior to characterization in CO–CO$_2$ atmosphere (20 h at $T = 800$ °C, $p\mathrm{H_2} = 8.6 \times 10^4$ Pa, $p\mathrm{H_2O} = 1.5 \times 10^4$ Pa, $p\mathrm{N_2} = 0$ Pa). The actual l_{TPB}

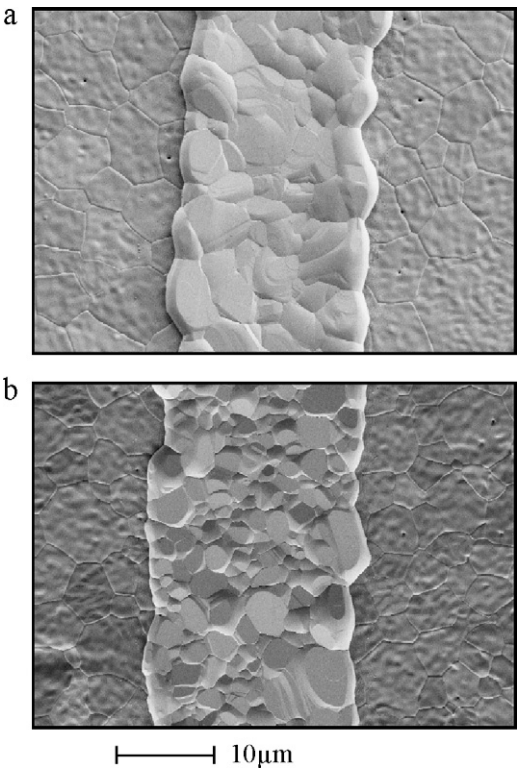

Fig. 5. SEM images of patterned Ni anodes: (a) after characterization at 800 °C for varying gas compositions of pH_2 and pH_2O and (b) gas compositions of pCO and pCO_2. The average increase in l_{TPB} is the same in both cases, $\tau_{corr} = 1.3$.

($l_{TPB,corr}$) is determined using the image processing tool SPIP [27]; the correction factor τ_{corr} being the quotient of $l_{TPB,corr}$ and the theoretical l_{TPB} ($l_{TPB,th}$). The average value determined for different positions on one sample as well as for several samples is almost constant and therefore taken as a standard value. Furthermore, the same value is obtained for patterned Ni anodes after characterization at 800 °C in H_2–H_2O atmosphere and CO–CO_2 atmosphere (see Fig. 5) which affirms that no further grain growth occurs after the initial heat treatment.

4.2. Relaxation and degradation processes

Applying the same standard initial heat treatment at 800 °C as for the characterization of Ni in H_2–H_2O atmosphere, the same initial decrease in LSR_{ct} was observed as already reported in our previous study [8]. Fig. 6 shows the relaxation behavior of patterned Ni anodes upon variation of the gas composition. Contrary to the long settling time upon variation of pH_2O and pH_2 with 2–3 h and more than 5 h respectively [8], equilibrium is attained fast in CO–CO_2 atmosphere. Furthermore, the observed degradation rate is less pronounced: at $pCO = 4.8 \times 10^4$ Pa and $pCO_2 = 5.4 \times 10^4$ Pa a degradation rate of 0.18% h^{-1} is determined, see Fig. 7.

One hypothesis for the explanation of the relaxation behavior in H_2–H_2O atmosphere is a slow settling of species concentration in the electrode or the electrolyte e.g. hydrogen atoms in Ni or interstitial protons in YSZ [3,8,28]. The absence of the slow relaxation in CO–CO_2 atmosphere may either indicate that no storage of interstitial species occurs or that the reaction proceeds following different reaction steps.

The lower degradation rate for CO–CO_2 compared to H_2–H_2O atmosphere affirms the hypothesis of degradation due to formation of gaseous $Ni(OH)_2$ [8,29]. However, in CO–CO_2 atmosphere the patterned Ni anode is still subject to degradation; this mechanism is not yet clear.

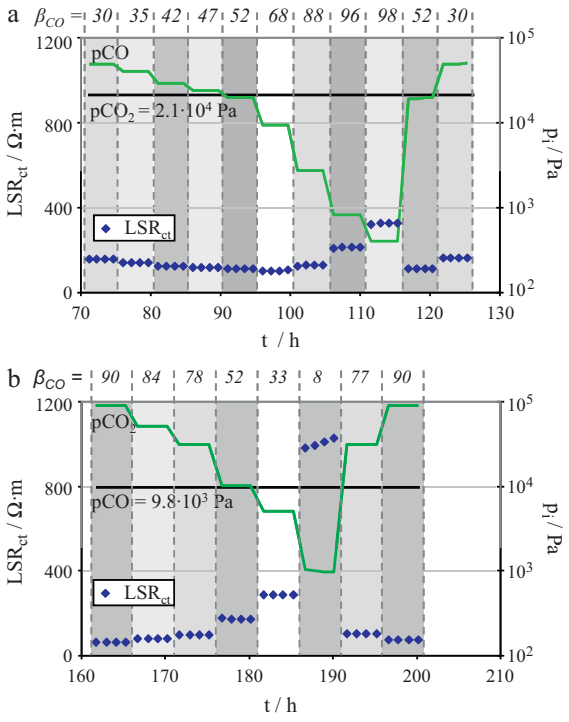

Fig. 6. Relaxation behavior of patterned Ni anodes for variation of (a) pCO with $pCO_2 = 2.1 \times 10^4$ Pa and (b) pCO_2 with $pCO = 9.8 \times 10^3$ Pa. Both are recorded at $T = 800$ °C, N_2 is used as balance gas ($l_{TPB,corr} = 1.3$ m).

4.3. Parameter dependencies

In the following, the results of data series recorded considering the before-mentioned degradation mechanisms are presented. The dependencies of LSR_{ct} on the parameters gas composition and temperature are determined in accordance to studies by our group [17,30] for Ni/8YSZ cermet anodes using the Butler–Volmer equation. The exchange current density j_0 is described by a power law Ansatz for the partial pressure dependencies of pCO and pCO_2 and an Arrhenius-type temperature dependency [31,32]:

$$j = j_0 \left[\exp\left(\alpha \frac{n_e F \eta_{ct}}{RT} \right) - \exp\left(-(1-\alpha) \frac{n_e F \eta_{ct}}{RT} \right) \right] \quad (4)$$

$$j_0 = \gamma (pCO)^c (pCO_2)^d \exp\left(-\frac{E_{act,ct}}{RT} \right) \quad (5)$$

Here, j_0 is the partial pressure and temperature dependent exchange current density, n_e the number of exchanged electrons

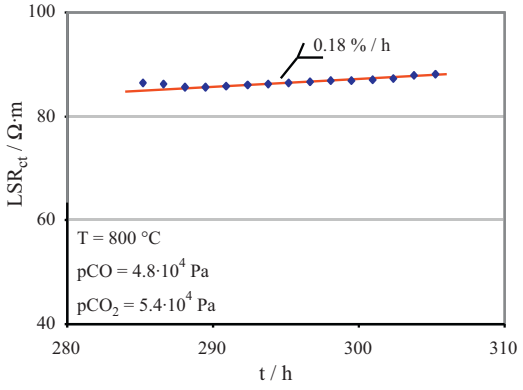

Fig. 7. Degradation behavior of patterned Ni anodes recorded at 800 °C for $pCO = 4.8 \times 10^4$ Pa and $pCO_2 = 5.4 \times 10^4$ Pa ($l_{TPB,corr} = 1.3$ m).

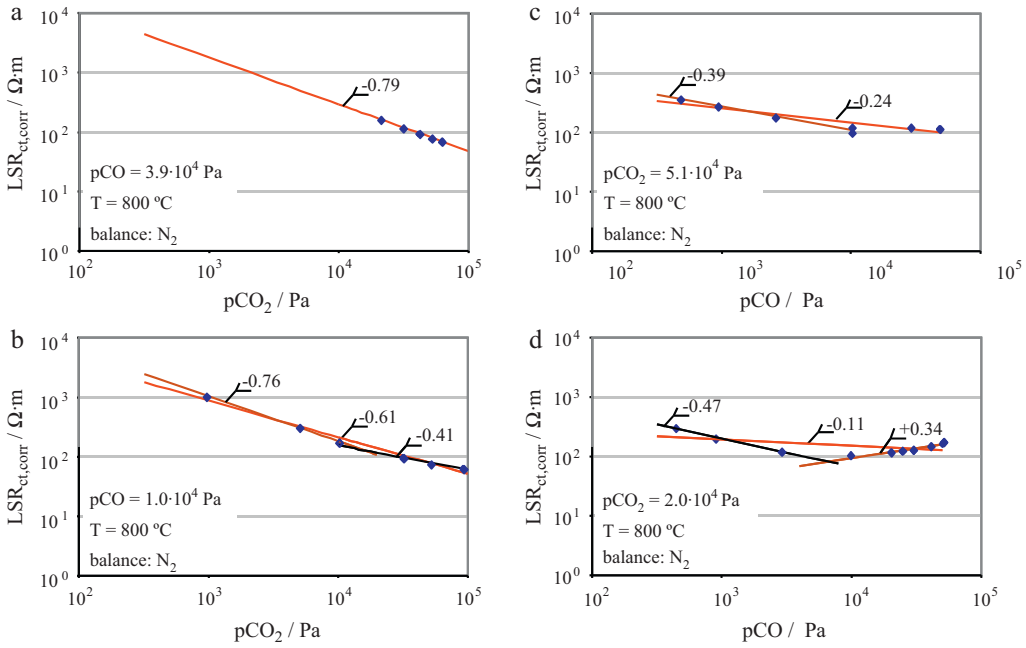

Fig. 8. Parameter dependency of LSR_{ct} as a function of pCO_2 (a, b) and pCO (c, d) at $T = 800\,^{\circ}C$, $l_{TPB,corr} = 1.3$ m. LSR_{ct} values are corrected for the degradation during recording of parameter variation yielding $LSR_{ct,corr}$.

(in our case $n_e = 2$), α the charge transfer coefficient and η_{ct} the activation overpotential.

In this study, the parameter dependencies of LSR_{ct} are determined based on the inverse proportionality of exchange current density and resistance ($LSR_{ct} \sim 1/j_0$) and are described by the exponents c and d (dependency of LSR_{ct} on pCO and pCO_2 respectively) and E_{act} (temperature dependency):

$$LSR_{ct} = c_3 \cdot (pCO)^{-c} \cdot (pCO_2)^{-d} \quad (6)$$

$$LSR_{ct} = c_4 \cdot \exp\left(\frac{E_{act,ct}}{RT}\right) \quad (7)$$

Fig. 8 shows the LSR_{ct} values obtained for a series of pCO and pCO_2 variation in a graph with double-logarithmic scale. The slopes of this graph correspond to the exponents $-c$ respectively $-d$ in Eq. (6). A strong dependency on pCO_2 is observable with $d = 0.79$ for $pCO = 3.9 \times 10^4$ Pa and $d = 0.61$ for $pCO = 1.0 \times 10^4$ Pa. In the latter case the dependency shows a kink at 2×10^4 Pa with higher slope ($d = 0.76$) for lower pCO_2 values and attenuated slope ($d = 0.41$) for higher pCO_2 values.

The dependency of LSR_{ct} on pCO is less pronounced: for $pCO_2 = 5.1 \times 10^4$ Pa a value of $c = 0.24$ is obtained; at $pCO_2 = 2.0 \times 10^4$ Pa inverse behaviors are found for low and high pCO values. For pCO inferior to 10^4 Pa LSR_{ct} decreases with increasing partial pressure ($c = 0.47$), whereas for higher pCO values LSR_{ct} increases with increasing pCO ($c = -0.34$).

The activation energy has been determined in the temperature range of 700–800 °C. For $pCO = 3.9 \times 10^4$ Pa and $pCO_2 = 4.2 \times 10^4$ Pa a value of 1.42 eV is obtained, see Fig. 9. Additionally, the activation energy in three operation points of pCO variation at $pCO_2 = 2.0 \times 10^4$ Pa (Fig. 8d) has been determined. A clear difference in activation energy is discernable for the three gas compositions between 0.85 eV and 1.42 eV with increasing activation energy for increasing pCO, see Fig. 10a). Fig. 10b shows the pCO dependency of LSR_{ct} for $T = 700$, 750, 800 °C at $pCO_2 = 2.0 \times 10^4$ Pa. The kink in dependency of LSR_{ct} on pCO at around $pCO = 2 \times 10^4$ Pa is reproducible for all temperatures.

Both, the changes in slope for the pCO dependency and the different activation energies indicate that different reaction mechanisms prevail in different regions of pCO–pCO_2 gas composition. For instance, a gas composition dependent co-limitation of several mechanisms is possible such as reported for the H_2 oxidation for different temperatures [3]. Fig. 11 gives an overview of the obtained gas dependencies and the activation energies as a function of pCO and pCO_2.

4.4. Comparison to related work

As stated above, little work is published that realized systematic parameter variation of one parameter at a time that allows determining quantitative parameter dependencies; among them is no study with patterned Ni anodes. Furthermore, a direct comparison of LSR data is difficult due to the different anode concepts of Ni grid electrode [11] and Ni/8YSZ cermet electrode [17]. However, a semi quantitative comparison is performed in this study. To that aim, the reported polarization resistances are taken from

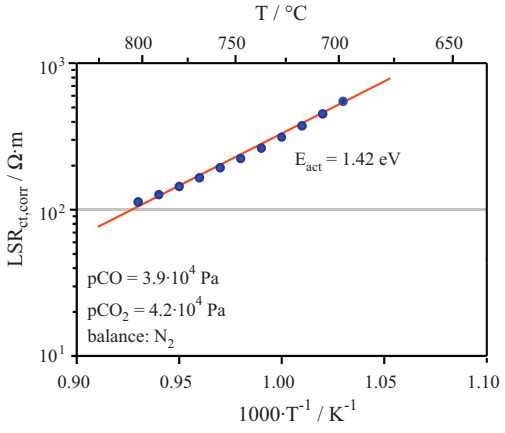

Fig. 9. Temperature dependency of LSR_{ct} recorded at $pCO = 3.9 \times 10^4$ Pa and $pCO_2 = 4.2 \times 10^4$ Pa, $l_{TPB,corr} = 1.3$ m. The activation energy is $E_{act,ct} = 1.42$ eV. LSR_{ct} values are corrected for the degradation during recording of parameter variation yielding $LSR_{ct,corr}$.

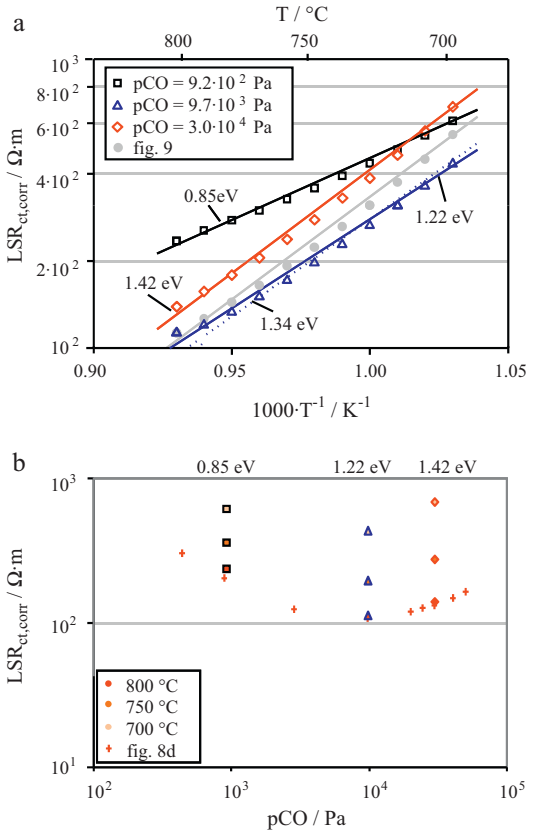

Fig. 10. (a) Temperature dependency of LSR_{ct} recorded for different pCO at $pCO_2 = 2.0 \times 10^4$ Pa together with the data points of Fig. 9, $l_{TPB,corr} = 1.3$ m. The activation energy varies considerably between $E_{act,ct} = 0.85$–1.42 eV. (b) LSR_{ct} as function of pCO for $T = 700$, 750,and 800 °C together with the data series at 800 °C from Fig. 8d, $pCO_2 = 2.0 \times 10^4$ Pa. Values are corrected for the degradation during recording of parameter variation yielding $LSR_{ct,corr}$.

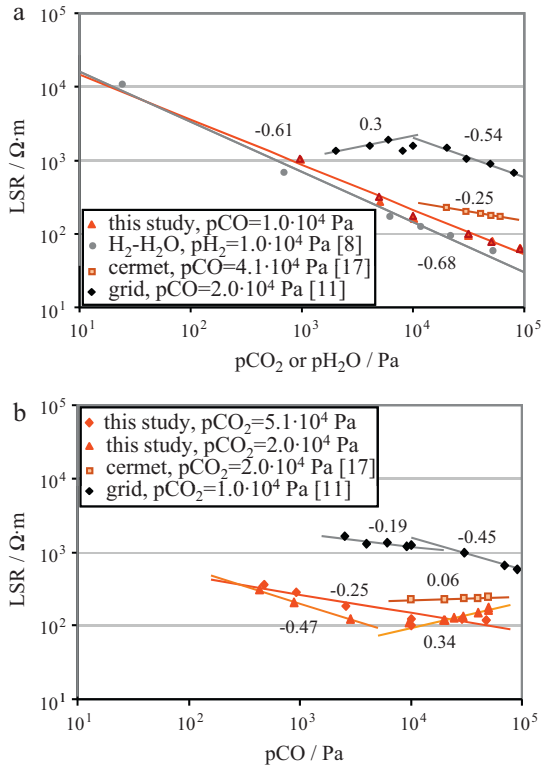

Fig. 12. Comparison of LSR_{ct} data from this study together with data by Boulenouar [11] for a Ni grid electrode (grid) and results of our group for anode supported Ni/8YSZ cermet electrodes (cermet) [17]. Note that results from Boulenouar are reported for 850 °C contrary to 800 °C for our studies. (a) Variation of pCO_2 and additional data points for pH_2O variation reported in our previous study [8], and (b) variation of pCO.

the respective studies and the triple phase boundary lengths (l_{TPB}) of both anodes are roughly estimated: assuming a reaction line at both sides of each Ni wire for the mesh with 400 mesh/in. we get a value of $l_{TPB} = 6.27$ m cm^{-2} for the Ni grid ($A = 0.071$ cm^2). For the Ni/8YSZ cermet electrode, l_{TPB} per volume values are taken from 3D reconstruction literature, that report values of percolating l_{TPB} between 2.7×10^{12} to 3.5×10^{12} m^{-2} [33] and 4.3×10^{12} to 5.4×10^{12} m^{-2} [34]. A mean value of $l_{TPB} = 4 \times 10^{12}$ m^{-2} is chosen for the calculation in this study. Multiplied with the thickness of the anode functional layer (AFL) of 7 μm this yields a value of $l_{TPB} = 2.8 \times 10^3$ m cm^{-2} ($A = 1$ cm^2).

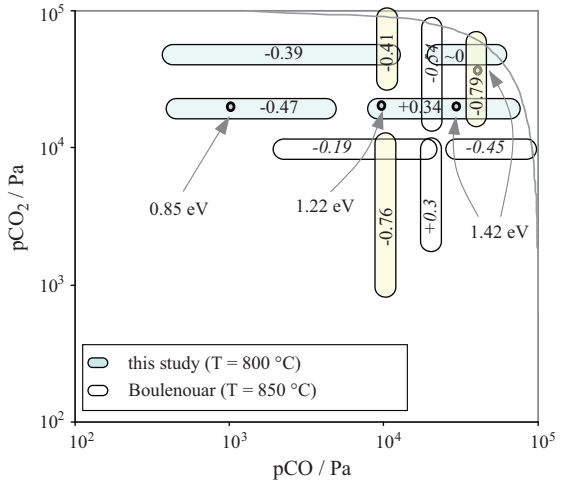

Fig. 11. Summary of parameter variation range of pCO and pCO_2 realized in this study together with the parameter dependencies of LSR_{ct} on pCO, pCO_2 and T ($-c$, $-d$ and $E_{act,ct}$). Additionally, results of the study of Boulenouar are indicated [11].

Fig. 12 shows all data points from Fig. 8 as well as the data extracted from literature as a function of pCO_2 and pCO respectively. Additionally, LSR_{ct} values of characterization of patterned anodes in H_2–H_2O atmosphere at 800 °C are included [8].

Comparing the pCO_2 dependency, the same trend is observed between data from our study ($d = 0.61$–0.79) and Boulenouar ($d = 0.54$) for values above 10^4 Pa, whereas at lower pCO_2 values Boulenouar reports a positive dependency with $d = -0.3$.

Comparing the pCO dependency no agreement is found: Boulenouar reported a negative dependency of LSR_{ct} on pCO throughout the investigated pCO range with $c = 0.19$–0.45; whereas in our study a kink in proportionality is observed for $pCO_2 = 2 \times 10^4$ Pa between negative proportionality for low pCO values ($c = 0.47$) and direct proportionality at higher pCO values ($c = -0.34$). No values for the activation energy are reported in the study of Boulenouar.

The comparison with the results from Ni/8YSZ cermet anodes shows similar dependencies: negative proportionality for pCO_2 as well as direct proportionality for high pCO values. In order to compare the quantitative values it must be considered that the polarization resistances of the cermet anode include both contributions of (i) oxygen ion transport in the YSZ matrix and (ii) charge transfer at the TPB [17,30,35]. The parameter dependencies reported in the study of our group with Ni/8YSZ cermet anodes are so-called apparent parameter dependencies.

Following the equation for the impedance of a transmission line model (Z_{TL}) and using the simplification of good conductivity in the Ni-matrix with negligible ohmic resistance one obtains [35–37]:

$$Z_{TL} = \lambda \cdot \chi_1 \cdot \coth\left(\frac{L}{\lambda}\right) \quad (8)$$

with

$$\lambda = \sqrt{\frac{\zeta}{\chi_1}} \quad (9)$$

In this context, χ_1 represents the oxygen ion conduction in the YSZ matrix; ζ represents the charge transfer at the TPB; L is the length of the transmission line and corresponds to the thickness of the anode functional layer; λ is the penetration depth. For direct current, the total resistances of the ionic path R_1 and the charge transfer R_3 are calculated from

$$R_1 = z_1 \cdot L = \chi_1 \cdot L \quad (10)$$

$$R_3 = \frac{z_3}{L} = \frac{\zeta}{L} \quad (11)$$

Considering a case distinction between charge transfer controlled and (ionic) transport controlled conditions we obtain the following results for the impedance of the transmission line model:

(i) $R_3 \gg R_1$ (charge transfer controlled):

$$Z_{TL} = \frac{1}{3}R_1 + R_3 \quad (12)$$

(ii) $R_1 \gg R_3$ (ionic transport controlled):

$$Z_{TL} = \sqrt{R_1 \cdot R_3} \quad (13)$$

A comparison of both regimes with experimental data from characterization of Ni/8YSZ cermet anodes indicates a tendency to transport controlled conditions with $R_1 \gg R_3$. Hence, the following relations apply for the parameter dependencies of gas composition and temperature:

(i) Under the assumption that ionic transport is independent of gas composition, and that the gas dependency of charge transfer follows Eq. (6) the transmission line impedance Z_{TL} is:

$$Z_{TL}(p\mathrm{CO}, p\mathrm{CO_2}) = \sqrt{R_1 \cdot R_3(p\mathrm{CO}, p\mathrm{CO_2})} \quad (14a)$$

$$Z_{TL}(p\mathrm{CO}, p\mathrm{CO_2}) = \sqrt{R_1 \cdot c_3} \cdot p\mathrm{CO}^{-c/2} \cdot p\mathrm{CO_2}^{-d/2} \quad (14b)$$

Hence, the apparent parameter dependencies $c_{app} = 0.5 \cdot c$ and $d_{app} = 0.5 \cdot d$ on pCO and pCO$_2$ respectively are attenuated compared to the parameter dependencies of the pure charge transfer process. With $d = 0.79$ in this study compared to $d_{app} = 0.25$ obtained for cermet anodes for pCO$_2$ variation as well as $c = -0.34$ in this study compared to $c_{app} = -0.06$ obtained for cermet anodes for pCO variation this prediction is not completely reproduced, though the tendency is right.

(ii) The apparent activation energy $E_{act,app}$ is calculated as the mean value of the activation energies of ionic transport E_{act,R_1} and charge transfer E_{act,R_3}:

$$E_{act,Z_{TL}} = \frac{E_{act,R_1} + E_{act,R_3}}{2} \quad (15)$$

The activation energy reported by our group for cermet anodes ($E_{act,app} = 1.23$ eV) is recorded at pCO $= 4.1 \times 10^4$ Pa and pCO$_2$ $= 6.1 \times 10^4$ Pa [17] and therefore in the same parameter region as the activation energy of $E_{act,ct} = 1.42$ eV reported in this study, see Fig. 11. Under the assumption of a constant contribution of ionic conduction for H_2–H_2O and CO–CO$_2$ atmosphere, the activation energy of ionic transport $E_{act,R_1} = 0.90$ eV is taken from the study of Sonn et al. [35]. Applying Eq. (15), an activation energy of charge transfer of $E_{act,ct} = 1.56$ eV (it is $E_{act,ct} = E_{act,R_3}$) is obtained with the data of cermet anodes.

The deviations in absolute LSR$_{ct}$ values of a factor of 2 compared to cermet anode data and a factor of 10 compared to grid electrode data are small taking into account the uncertainty in estimating the triple phase boundary length. For the Ni/8YSZ cermet the uncertainty makes up about a factor of ±1.4 and for the Ni grid electrode a factor of −2. Especially the good agreement between the results from this study and the results from characterization of Ni/8YSZ cermet anodes is promising and encourages performing further comparative studies between characterization results of cermet and patterned anodes.

Fig. 12a additionally includes LSR$_{ct}$ values determined in our study with patterned Ni anodes in H_2–H_2O atmosphere [8]. LSR$_{ct}$ values of characterization in CO–CO$_2$ atmosphere exhibit only slightly higher polarization losses for the CO oxidation than the H_2 oxidation of less than a factor of 2. This indicates that the reaction mechanisms of H_2 and CO oxidation proceed in a similar way. A complete blocking of the TPB by impurities and a reaction exclusively by diffusion of protons in the Ni as discussed by Mogensen and co-workers [38,39] seems rather improbable in this context as diffusion of CO in Ni is very limited.

5. Conclusions

The characterization of patterned Ni anodes has been extended from H_2–H_2O atmosphere to the investigation of the CO oxidation in CO–CO$_2$ atmosphere. The variation of pCO, pCO$_2$ and T was realized in a large parameter range under avoidance of NiO and coke formation.

Special focus was directed to stability as well as relaxation and degradation processes:

(i) The stability of the patterned Ni anodes was controlled by pre- and post-test SEM analysis: the same increase in l_{TPB} ($\tau_{corr} = 1.3$) due to grain growth was observed than for the characterization in H_2–H_2O atmosphere.

(ii) No slow relaxation processes with time constants in the hour – scale as observed for H_2–H_2O atmospheres (2–5 h) were observable upon changes in the gas composition of CO–CO$_2$.

(iii) The degradation rate was determined to 0.18% h^{-1} (pCO $= 4.8 \times 10^4$ Pa, pCO$_2$ $= 5.4 \times 10^4$ Pa) which is less pronounced compared to the degradation rates previously determined for patterned Ni anodes in H_2–H_2O atmosphere of 0.4% h^{-1}.

Parameter dependencies have been determined for variation of pCO, pCO$_2$ and T individually. A negative dependency was found for LSR$_{ct}$ on pCO$_2$ variations with $d = 0.61$–0.79. A change in dependency of LSR$_{ct}$ on pCO was found between negative proportionality for pCO $< 2 \times 10^4$ Pa and direct proportionality for higher pCO values. This observation together with distinct activation energies between $E_{act,ct} = 0.85$–1.42 eV is interpreted as an indicator for changes in the reaction mechanism.

The comparison to results previously determined for Ni/8YSZ cermet anodes yields good agreement. The small deviation in absolute LSR values of a factor of 2 is mainly attributed to uncertainties in the estimation of the triple phase boundary length of the cermet anode (factor of ±1.4).

Slightly higher absolute LSR$_{ct}$ values are obtained for the characterization in CO–CO$_2$ atmosphere than in H_2–H_2O (deviation less than a factor of 2). This renders a limiting reaction mechanisms involving proton diffusion in the Ni electrode improbable.

Acknowledgements

The authors like to thank Dr. H. Störmer (Laboratorium für Elektronenmikroskopie (LEM), KIT) for the preparation and microstructural analysis of patterned Ni anodes as well as Dr. W. Bessler and his group at DLR Stuttgart for collaboration.

Funding by the German Research Foundation (DFG), project WE 4188/1-1, is gratefully acknowledged.

References

[1] A. Atkinson, S.A. Barnett, R.J. Gorte, J.T.S. Irvine, A.J. McEvoy, M. Mogensen, S.C. Singhal, Nat. Mater. 3 (2004) 17–27.
[2] S.B. Adler, W.G. Bessler, in: W. Vielstich, H. Yokokawa, H.A. Gasteiger (Eds.), Handbook of Fuel Cells—Fundamentals, Technology and Applications, John Wiley & Sons Ltd, Chichester, 2009, pp. 441–462.
[3] W.G. Bessler, M. Vogler, H. Störmer, D. Gerthsen, A. Utz, A. Weber, E. Ivers-Tiffée, Phys. Chem. Chem. Phys. (2010), doi:10.1039/C0CP00541J.
[4] A. Bieberle, L.P. Meier, L.J. Gauckler, J. Electrochem. Soc. 148 (2001) A646–A656.
[5] B. de Boer, PhD Thesis, University of Twente, Twente, Netherlands, 1998.
[6] J. Mizusaki, H. Tagawa, T. Saito, T. Yamamura, K. Kamitani, K. Hirano, S. Ehara, T. Takagi, T. Hikita, M. Ippommatsu, S. Nakagawa, K. Hashimoto, Solid State Ionics 70 (1994) 52–58.
[7] J. Mizusaki, H. Tagawa, T. Saito, K. Kamitani, T. Yamamura, K. Hirano, S. Ehara, T. Takagi, T. Hikita, M. Ippommatsu, S. Nakagawa, K. Hashimoto, J. Electrochem. Soc. 141 (1994) 2129–2134.
[8] A. Utz, H. Störmer, A. Leonide, A. Weber, E. Ivers-Tiffée, J. Electrochem. Soc. 157 (2010) B920–B930.
[9] M. Vogler, A. Bieberle-Hutter, L. Gauckler, J. Warnatz, W.G. Bessler, J. Electrochem. Soc. 156 (2009) B663–B672.
[10] R.J. Aaberg, R. Tunold, S. Tjelle, R. Odegard, Proceedings of the 17th Risoe International Symposium on Materials Science: High Temperature Electrochemistry:Ceramics and Metals, 1996, pp. 511–516.
[11] F.Z. Boulenouar, K. Yashiro, M. Oishi, A. Kaimai, Y. Nigara, T. Kawada, J. Mizusaki, Electrochem. Soc. Ser. 2001 (2001) 759–768.
[12] K. Eguchi, T. Setoguchi, K. Okamoto, H. Arai, ECS Trans. 93 (4) (1993) 494–503.
[13] T.H. Etsell, S.N. Flengas, J. Electrochem. Soc. 118 (1971) 1890–1900.
[14] P. Holtappels, L.G.J. de Haart, U. Stimming, I.C. Vinke, M. Mogensen, J. Appl. Electrochem. 29 (1999) 561–568.
[15] G.O. Lauvstad, R. Tunold, S. Sunde, J. Electrochem. Soc. 149 (2002) E506–E514.
[16] J. Mizusaki, H. Tagawa, Y. Miyaki, S. Yamauchi, K. Fueki, I. Koshiro, K. Hirano, Solid State Ionics 53 (6) (1992) 126–134.
[17] A. Leonide, S. Hansmann, A. Weber, E. Ivers-Tiffée, J. Power Sources (2010), doi:10.1016/j.jpowsour.2010.10.052.
[18] T. Setoguchi, K. Okamoto, K. Eguchi, H. Arai, J. Electrochem. Soc. 139 (1992) 2875–2880.
[19] A. Weber, B. Sauer, A.C. Müller, D. Herbstritt, E. Ivers-Tiffée, Solid State Ionics 152 (2002) 543–550.
[20] A.M. Sukeshini, B. Habibzadeh, B.P. Becker, C.A. Stoltz, B.W. Eichhorn, G.S. Jackson, J. Electrochem. Soc. 153 (2006) A705–A715.
[21] G.O. Lauvstad, R. Tunold, S. Sunde, J. Electrochem. Soc. 149 (2002) E497–E505.
[22] H.J. Levinson, W.H. Arnold, in: P. Rai-Choudhury (Ed.), Handbook of Microlithography, Micromachining and Microfabrication, SPIE—The International Society of Optical Engineering, Bellingham,WA, 1997, pp. 11–138.
[23] A. Utz, H. Störmer, D. Gerthsen, A. Weber, E. Ivers-Tiffée, Solid State Ionics (2010), doi:10.1016/J.SSI.2010.05.004.
[24] S.B. Adler, J. Electrochem. Soc. 149 (2002) E166–E172.
[25] E. Ivers-Tiffée, H. Timmermann, A. Leonide, N.H. Menzler, J. Malzbender, in: W. Vielstich, H. Yokokawa, H.A. Gasteiger (Eds.), Handbook of Fuel Cells—Fundamentals, Technology and Applications, John Wiley & Sons Ltd, Chichester, 2009, pp. 933–956.
[26] MALT—MAterials-oriented Little Thermodynamic Database, Version 1.0, Kagaku Gijutsu-Sha, 2004.
[27] SPIP Scanning Probe Image Processor, Version 4.0, Image Metrology A/S, 1998.
[28] D. Kek, M. Mogensen, S. Pejovnik, J. Electrochem. Soc. 148 (2001) A878–A886.
[29] R. Stübner, PhD Thesis, Technische Universität Dresden, Dresden, Germany, 2002.
[30] A. Leonide, Y. Apel, E. Ivers-Tiffee, ECS Trans. 19 (2009) 81–109.
[31] A.J. Bard, L.R. Faulkner, Electrochemical Methods: Fundamentals and Applications, John Wiley & Sons, New York, 2001.
[32] H. Wendt, G. Kreysa, Electrochemical Engineering, Springer, Berlin, 1999.
[33] J.R. Wilson, W. Kobsiriphat, R. Mendoza, H.Y. Chen, J.M. Hiller, D.J. Miller, K. Thornton, P.W. Voorhees, S.B. Adler, S.A. Barnett, Nat.Mater. 5 (2006) 541–544.
[34] P.R. Shearing, J. Golbert, R.J. Chater, N.P. Brandon, Chem. Eng. Sci. 64 (2009) 3928–3933.
[35] V. Sonn, A. Leonide, E. Ivers-Tiffée, J. Electrochem. Soc. 155 (2008) B675–B679.
[36] J. Bisquert, G.G. Belmonte, F.F. Santiago, N.S. Ferriols, M. Yamashita, E.C. Pereira, Electrochem. Commun. 2 (2000) 601–605.
[37] G. Paasch, K. Micka, P. Gersdorf, Electrochim. Acta 38 (1993) 2653–2662.
[38] M. Mogensen, K.V. Hansen, in: W. Vielstich, H. Yokokawa, H.A. Gasteiger (Eds.), Handbook of Fuel Cells—Fundamentals, Technology and Applications, John Wiley & Sons Ltd, Chichester, 2009, pp. 543–554.
[39] M.S. Schmidt, K.V. Hansen, K. Norrman, M. Mogensen, Solid State Ionics 179 (2008) 2290–2298.